Journal of Magnetism and Magnetic Materials 364 (2014) 55–59

Contents lists available at ScienceDirect

Journal of Magnetism and Magnetic Materials

journal homepage: www.elsevier.com/locate/jmmm

Magnetization pole reversal of ferrimagnetic ludwigites $Mn_{3-x}Ni_xBO_5$

L.N. Bezmaternykh, E.M. Kolesnikova *, E.V. Eremin, S.N. Sofronova, N.V. Volkov, M.S. Molokeev

Kirensky Institute of Physics, Russian Academy of Sciences, Siberian Branch, Akademgorodok 50, Building 38, Krasnoyarsk 660036, Russia

ARTICLE INFO

Article history:
Received 20 January 2014
Received in revised form
7 April 2014
Available online 18 April 2014

Keywords:
Ferrimagnets
Magnetization pole reversal
Crystal growth

ABSTRACT

The conditions for the flux growth of new Mn–Ni oxyborates with the ludwigite structure are reported. Magnetic measurement data for the samples with nickel and manganese predominance are presented. Magnetization pole reversal of the ferrimagnetic phases is established and analyzed in the framework of a model comprising two antiferromagnetically interacting subsystems, each being ferrimagnetically ordered.

1. Introduction

Magnetization pole reversal at cooling or heating of ferrimagnets with different crystal-chemical characteristics has been known since long time ago [1–10]. All the scenarios are quite similar. Upon cooling the samples in medium magnetic field (FC) magnetization decreases starting from some temperature $T<T_N$, then it passes through the compensation point ($M=0$) and after that it begins to grow in the opposite direction of the applied magnetic field. If the sample is cooled in zero magnetic field (ZFC), then at switching on of the magnetic field first its magnetization is directed along the field. As the temperature is increased the magnetization decreases, passing through a new compensation point. After that it becomes negative and again changes the sign near T_N.

Such behavior of the magnetization is described in the frameworks of a model comprising two antiferromagnetically interacting subsystems, each being ferrimagnetically ordered, which has different temperature dependences on magnetization, as shown in [10]. Spin–lattice interaction is the main factor, determining difference of temperature dependences of subsystems magnetization. The peculiarities of spin–lattice interaction, in the case of $NdMnO_{3.11}$, could be related with the presence of both Mn^{3+} and Mn^{4+} cations [5], and, in the case of $Ni(HCOO)_2\cdot 2H_2O$, it could be related with two-position distribution of Ni^{2+} cations [10].

Recently [11], another scenario of magnetization pole reversal was observed in ludwigite $Mn_{2.25}Co_{0.75}BO_5$ with heterovalent Mn- and Co- subsystems and quasi-two-dimensional distribution of magnetoactive cations. In ZFC regime, the sample magnetization is in the direction opposite to the applied magnetic field.

To sum up, the contemporary existing experimental data as well as the models developed are still insufficient for systematization and, moreover, forecasting the above-mentioned phenomena depending on the crystal-chemical parameters of involved ferrimagnets cannot be done.

The aim of this study was to investigate magnetism of the new Mn-heterovalent ludwigites $Mn_{3-x}Ni_xBO_5$ ($0<x<3$) with different cations contents characterized by different spin–orbit couplings. A unique sample of compound in this family with $x=2.5$ was synthesized by Bluhm and Müller-Buschbaum [12], but its magnetic properties have not been studied yet. In this paper we report the magnetization data for the samples with low ($x_1=0.5$) and high ($x_2=1.8$) Ni concentration. We compare the temperature and the field evolutions of the ferrimagnetic phases in these samples and discuss the possibility of their description within one model comprising two antiferromagnetically interacting subsystems, each being ferrimagnetically ordered.

2. Crystal growth

$Mn_{2.5}Ni_{0.5}BO_5$ ($x_1=2.5$ and $n_1=15\%$) and $Mn_{1.2}Ni_{1.8}BO_5$ ($x_2=1.2$ and $n_2=7\%$) single crystals were synthesized from the fluxes

$$(100-n)\%\ \text{mass.}(Bi_2Mo_3O_{12}+0.6\ B_2O_3+0.7\ Na_2O)+$$
$$+n\%\ \text{mass.}\left(\frac{(3-x)}{2}Ni_2O_3+\frac{x}{2}Mn_2O_3+0.5B_2O_3\right)$$

The fluxes in a mass of 50–80 g were prepared from initial trioxides Mn_2O_3 and Ni_2O_3 in combination with sodium carbonate at the temperature $T=1100\ ^\circ C$ in a platinum crucible with the

* Corresponding author. Tel.: +7 391 243 26 35; fax: +7 391 243 89 23.
E-mail address: ekoles@iph.krasn.ru (E.M. Kolesnikova).

http://dx.doi.org/10.1016/j.jmmm.2014.04.031
0304-8853/

volume $V=100\ cm^3$ by sequential melting of powder mixtures, first $Bi_2Mo_3O_{12}$ and B_2O_3, then Mn_2O_3 and Ni_2O_3; finally, Na_2CO_3 was added in portions.

In the prepared fluxes, the phase crystallizing within a sufficiently wide (about 40 °C) high-temperature range was $Mn_{3-x}Ni_xBO_5$ with the ludwigite structure. The saturation temperatures of the fluxes were $T_{sat1}=920$ °C and $T_{sat2}=960$ °C.

Single crystals of the ludwigites were synthesized by spontaneous nucleation. After homogenization of the fluxes at $T=1100$ °C for 3 h, the temperature was first rapidly reduced to $T_{sat}-10$ °C and then slowly reduced at a rate of 2–4 °C/day. In 3 days, the growth was completed, the crucible was withdrawn from the furnace, and the flux was poured out. The grown single crystals in the form of orthogonal prisms with a length of 10 mm and a transverse size of about 0.5 mm were etched in a 20% water solution of nitric acid to remove the flux remainder.

3. Structural data

X-ray investigations of the $Mn_{2.5}Ni_{0.5}BO_5$ single crystal and $Mn_{1.2}Ni_{1.8}BO_5$ powder were carried out on a SMART APEXII diffractometer (Mo Kα, $\lambda=0.7106$ Å) at room temperature. The obtained data are given in Table 1. Both $Mn_{2.5}Ni_{0.5}BO_5$ and $Mn_{1.2}Ni_{1.8}BO_5$ samples belong to the space group *Pbam* (D_{2h}^9), i.e., have the ludwigite structure. The structure was refined by the least-square minimization using SHELX97 [13]. The unit cell involves four formula units, i.e., contains 12 magnetic atoms occupying 4 nonequivalent positions: 4g, 4h, 2a, and 2d. The ludwigite structure is presented in Fig. 1. We investigated

Table 1
Crystallographic data and main processing and refinement parameters for $Mn_{2.5}Ni_{0.5}BO_5$ and $Mn_{1.2}Ni_{1.8}BO_5$.

Crystallographic data		
Chemical formula	$Mn_{2.5}Ni_{0.5}BO_5$	$Mn_{1.2(1)}Ni_{1.8(1)}BO_5$
M_r	257.51	261.49
Space group, Z	*Pbam*, 4	*Pbam*, 4
a (Å)	9.179(2)	9.187(1)
b (Å)	12.344(2)	12.322(1)
c (Å)	3.0010(6)	3.0010(3)
V (Å^3)	340.0(1)	339.71(6)
D_x (Mg/m^3)	5.030	5.113
μ (mm^{-1})	11.769	13.952
Size	$0.1\times0.1\times0.5$ mm^3	$0.1\times0.1\times0.5$ mm^3
Data collection		
Wavelength	Mo Kα, $\lambda=0.7106$ Å	Mo Kα, $\lambda=0.7106$ Å
Measured reflections	3107	3092
Independent reflections	546	546
Reflections with $I>2\sigma(I)$	514	503
Absorption correction	Multiscan	Multiscan
R_{int}	0.0409	0.0406
$2\theta_{max}$ (deg))	59.28	59.08
h	−12→12	−12→12
k	−17→16	−16→16
l	−4→4	−4→4
Refinement		
$R[F^2>2\sigma(F^2)]$	0.0381	0.0306
$wR(F^2)$	0.1112	0.0711
S	1.007	1.039
Weight	$w=1/[\sigma^2(F_o^2)+(0.00744P)^2+2.63P]$ where $P=\max(F_o^2+2F_c^2)/3$	$w=1/[\sigma^2(F_o^2)+(0.0457P)^2+102P]$ where $P=\max(F_o^2+2F_c^2)/3$
$(\Delta/\sigma)_{max}$	<0.07	<0.01
$\Delta\rho_{max}$ (e/Å^3)	1.77	1.02
$\Delta\rho_{min}$ (e/Å^3)	−1.50	−1.00
Extinction correction coefficient (SHELX97)	0.098(8)	0.062(4)

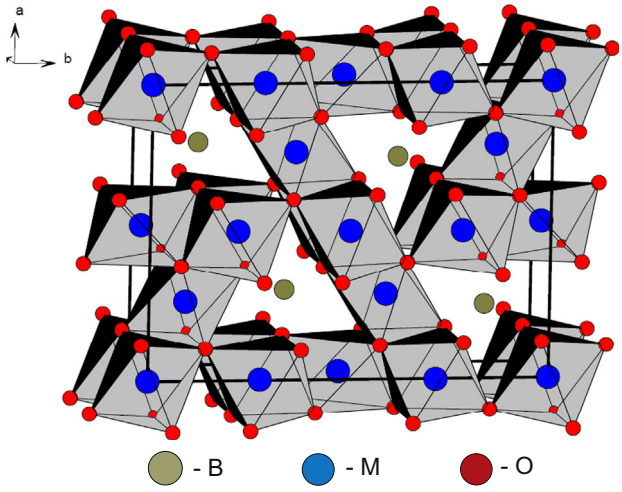

Fig. 1. Ludwigite structure (B—boron; M—transition metal (Mn or Ni); and O—oxygen).

Table 2
Fractional atomic coordinates and isotropic or equivalent isotropic displacement parameters (Å^2) for $Mn_{2.5}Ni_{0.5}BO_5$.

	Wyck.	*x*	*y*	*z*	U_{iso}*/U_{eq}	Occ.
Mn1	4g	−0.00269(8)	0.71967 (7)	0.0000	0.0096(3)	0.50
Ni1	4g	−0.00269(8)	0.71967 (7)	0.0000	0.0096(3)	0.50
Mn2	2a	0.0000	1.0000	0.0000	0.0046(4)	1
Mn3	4h	0.25977(9)	0.61538(7)	−0.5000	0.0069(3)	1
Mn4	2d	0.0000	0.5000	−0.5000	0.0050(4)	1
O1	4g	−0.1067(5)	0.8564(3)	0.0000	0.0166(10)	1
O2	4h	0.1449(4)	0.7642(4)	−0.5000	0.0149(9)	1
O3	4g	0.1128(5)	0.5796(4)	0.0000	0.0167(9)	1
O4	4h	−0.1272(5)	0.6416(3)	−0.5000	0.0129(9)	1
O5	4h	0.1477(5)	0.9582(3)	−0.5000	0.0142(9)	1
B	4h	0.2225(8)	0.8618(5)	−0.5000	0.0116(13)*	1

Table 3
Fractional atomic coordinates and isotropic or equivalent isotropic displacement parameters (Å^2) for $Mn_{1.2(1)}Ni_{1.8(1)}BO_5$.

	Wyck.	*x*	*y*	*z*	U_{iso}*/U_{eq}	Occ.
Ni1	4g	−0.00214(5)	0.78052(5)	0.0000	0.0071(3)	0.68(4)
Mn1	4g	−0.00214(5)	0.78052(5)	0.0000	0.0071(3)	0.31(4)
Ni2	2a	0.0000	0.5000	0.0000	0.0071(3)	0.69(4)
Mn2	2a	0.0000	0.5000	0.0000	0.0071(3)	0.31(4)
Ni3	4h	0.26000(6)	0.88485(5)	−0.5000	0.0069(2)	0.34(4)
Mn3	4h	0.26000(6)	0.88485(5)	−0.5000	0.0069(2)	0.66(4)
Ni4	2d	0.0000	1.0000	−0.5000	0.0076(3)	0.69(5)
Mn4	2d	0.0000	1.0000	−0.5000	0.0076(3)	0.31(5)
O1	4g	−0.1066(3)	0.6436(2)	0.0000	0.0129(7)	1
O2	4h	0.1129(3)	0.9209(3)	0.0000	0.0138(7)	1
O3	4g	0.1471(3)	0.7363(2)	−0.5000	0.0118(7)	1
O4	4h	−0.1264(3)	0.8588(2)	−0.5000	0.0105(7)	1
O5	4h	0.1475(3)	0.5421(2)	−0.5000	0.0112(7)	1
B1	4h	−0.2765(6)	0.8608(4)	−0.5000	0.0104(10)*	1

occupation of the crystallographic positions in $Mn_{2.5}Ni_{0.5}BO_5$ by magnetic atoms and showed that the positions 4h, 2a, and 2d are occupied only by Mn. Nickel and manganese ions together occupy the 4g position in $Mn_{2.5}Ni_{0.5}BO_5$; however, we failed to calculate the occupancies of this position by each ion because of the similarity of their atomic functions (Table 2). In $Mn_{1.2}Ni_{1.8}BO_5$, all the crystallographic positions are occupied by Ni and Mn ions; their refined occupancies are given in Table 3.

4. Magnetic characterization

Magnetic properties of the $Mn_{2.5}Ni_{0.5}BO_5$ single crystal and the $Mn_{1.2}Ni_{1.8}BO_5$ sample consisting of several *c*-axis-oriented crystals were measured on a PPMS-9 Physical Property Measurement System (Quantum Design) at the temperatures $T=3$–300 K in the magnetic fields $H=0.1$–80 kOe.

Temperature dependences of magnetization for the investigated samples are presented in Figs. 2 and 3. The dependences were obtained upon cooling the sample in the magnetic field $H=1$ kOe (FC) parallel ($H\|c$) or orthogonal ($H\perp c$) to the *c* axis. The magnetization of the $Mn_{2.5}Ni_{0.5}BO_5$ crystal (Fig. 2) monotonically increases below $T_N=81$ K at $H\perp c$. In the case $H\|c$, the temperature range of the magnetization variation is much narrower. Presumably, near $T_N=81$ K the phase transition from the paramagnetic to ferrimagnetic state occurs, which is related to alignment of the magnetic moments in the planes perpendicular to the *c* axis. The slow magnetization growth near T_N can result from the almost collinear alignment of the magnetic moments in this region. The temperature dependence of the inverse susceptibility $\chi_\perp^{-1}=H_\perp/M$ illustrated in the inset of Fig. 2 indicates predominance of the antiferromagnetic interaction. According to this dependence, the paramagnetic Curie temperature is negative: $\theta=-40$ K. In the paramagnetic phase, no magnetic anisotropy was found.

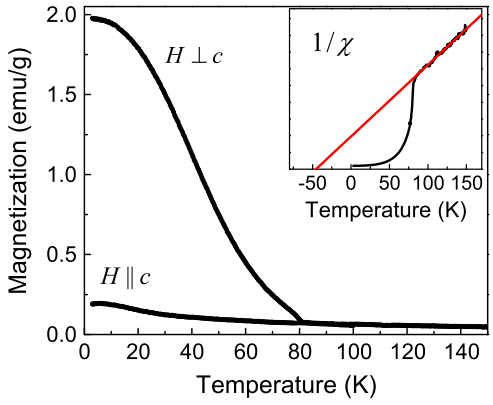

Fig. 2. Temperature dependencies of magnetization of $Mn_{2.5}Ni_{0.5}BO_5$ at different orientations of magnetic field ($H=1$ kOe; $H\perp c$, $H\|c$). Inset: temperature dependence of inverse susceptibility $\chi_\perp^{-1}$ (black line) and its linear extrapolation of paramagnetic area (red line). (For interpretation of the references to color in this figure legend, the reader is referred to the web version of this article.)

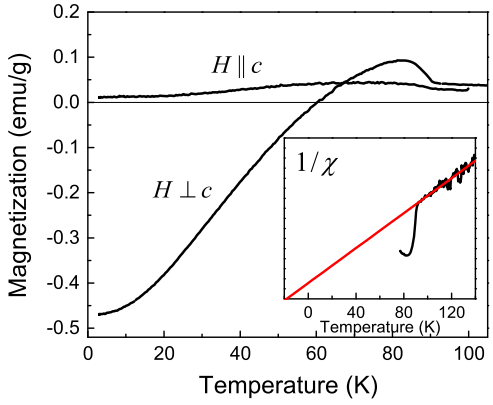

Fig. 3. Temperature dependences of magnetization of $Mn_{1.2}Ni_{1.8}BO_5$ at different orientations of magnetic field ($H=1$ kOe; $H\perp c$, $H\|c$). Inset: temperature dependency of inverse susceptibility $\chi_\perp^{-1}$ (black line) and its linear extrapolation to paramagnetic phase (red line). (For interpretation of the references to color in this figure legend, the reader is referred to the web version of this article.)

The paramagnetic Curie temperature of the $Mn_{1.2}Ni_{1.8}BO_5$ sample (Fig. 3) is also negative. The ferrimagnetic ordering temperature $T_N=92$ K was estimated from the temperature dependence of the magnetization obtained with $H\perp c$. The rapid growth of *M* near T_N can be attributed to the noncollinear alignment of the magnetic moments. Minor variations in *M* for $H\|c$ indicate that the spin–lattice interaction fixes the magnetic moments in the planes perpendicular to the *c* axis. The magnetic moments tend to orient in this way already in the paramagnetic phase.

Another important peculiarity of the temperature dependence of the magnetization for the $Mn_{1.2}Ni_{1.8}BO_5$ sample with $H\perp c$ is the presence of the compensation point $M=0$. Below this point, the magnetization is negative. As the temperature is decreased, the absolute value of the magnetization increases. Such an anomaly of the ferrimagnetic phase can be considered as magnetization pole reversal.

In the other regime (ZFC), temperature dependences of the magnetization were obtained upon sample heating after zero field cooling. The ZFC and FC dependences obtained with $H\perp c$ for two samples strongly differ (Fig. 4a and b).

In the ZFC regime, the $Mn_{2.5}Ni_{0.5}BO_5$ sample passes to the state with negative magnetization with switching on of the magnetic field (Fig. 4a). As the temperature is increased, the absolute value of the magnetization decreases. At certain temperature T_{cr}, the magnetic moment reverses and the sample undergoes a transition to the state obtained in the FC regime. With increasing magnetic field *H*, T_{cr} decreases (Fig. 5). In strong magnetic fields, the ZFC and FC dependences coincide. These measurements revealed the existence of two possible states of the ferrimagnetic phase in the $Mn_{2.5}Ni_{0.5}BO_5$ sample. The bistability is confirmed by the magnetic field dependences of the magnetization at different temperatures (Fig. 6). The temperature dependence of coercivity H_c is consistent with the field dependence of critical temperature T_{cr} (Fig. 7). Therefore, the key role in the formation of these two states is played by the spin–lattice interaction.

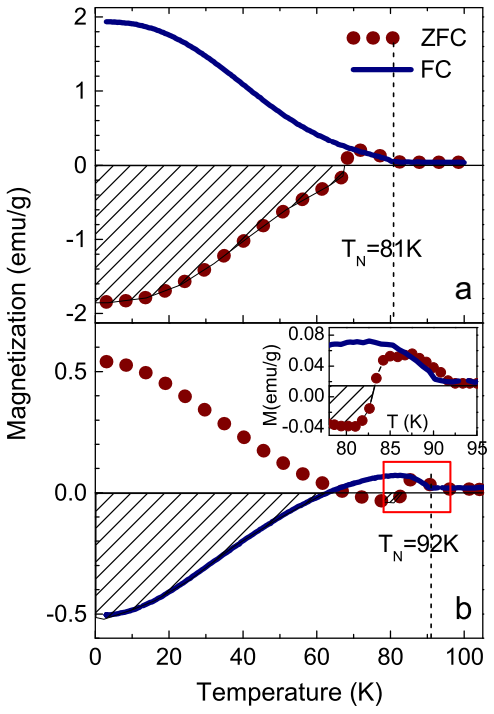

Fig. 4. Temperature FC- and ZFC-dependences of magnetization measured at $H=0.5$ kOe, $H\perp c$ (a—$Mn_{2.5}Ni_{0.5}BO_5$; and b—$Mn_{1.2}Ni_{1.8}BO_5$).

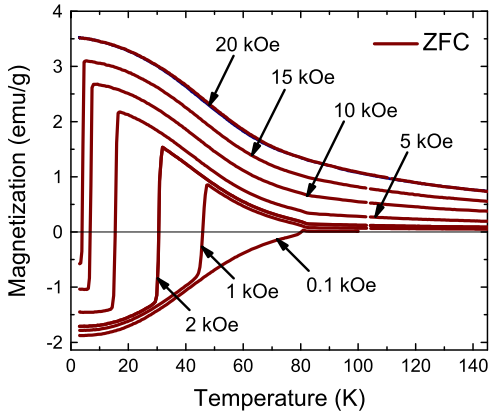

Fig. 5. Temperature ZFC-dependences of magnetization of $Mn_{2.5}Ni_{0.5}BO_5$ measured at different magnetic fields, $H \perp c$.

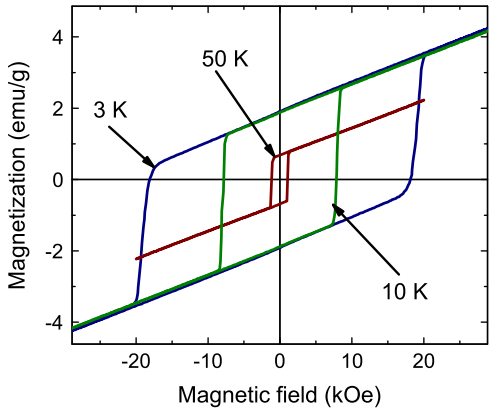

Fig. 6. Magnetic field dependences of magnetization of $Mn_{2.5}Ni_{0.5}BO_5$ measured at different temperatures ($H \perp c$).

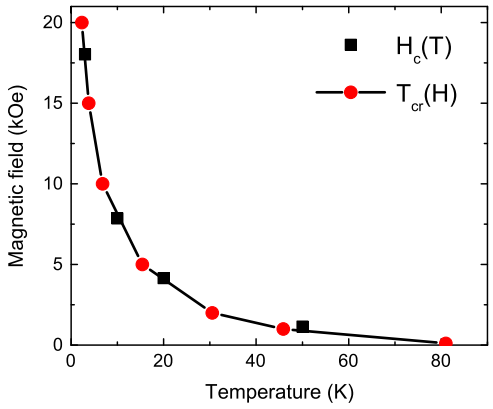

Fig. 7. Temperature dependence of coercitive field H_c (squares) and dependence of critical temperature T_{cr} (circles) of magnetic field of $Mn_{2.5}Ni_{0.5}BO_5$.

It should be noted that when at $H \| c$ the magnetic hysteresis is not observed (Fig. 8).

The magnetic behavior of $Mn_{2.5}Ni_{0.5}BO_5$ described within the model of two antiferromagnetically interacting subsystems can be explained as follows. Subsystem M_I is characterized by the stronger spin–lattice coupling, i.e., the higher coercivity, but its magnetic-field-induced magnetization is lower than that in subsystem M_{II}; subsystem M_{II} is "softer". Due to the strong antiferromagnetic interaction of these subsystems in weak fields, the sample can be in one of the two possible states: with the resulting induced moment $M=M_{II}-M_I$ directed either along the magnetic

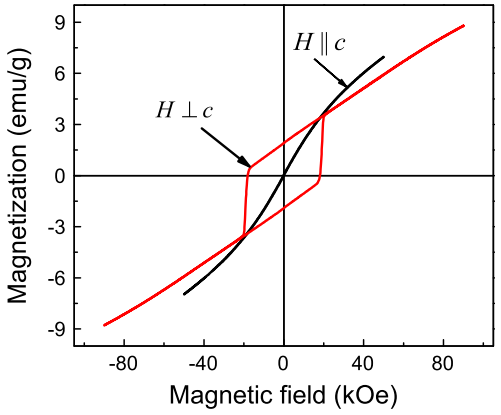

Fig. 8. Magnetic field dependences of magnetization of $Mn_{2.5}Ni_{0.5}BO_5$ measured at $H \perp c$ and $H \| c$ ($T=3$ K).

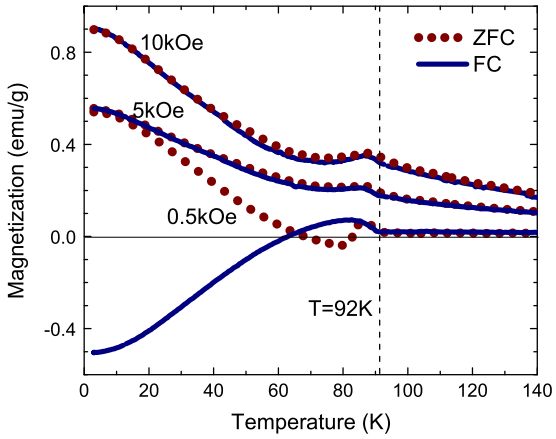

Fig. 9. Temperature FC- and ZFC-dependences of magnetization of $Mn_{1.2}Ni_{1.8}BO_5$ measured at different magnetic fields ($H \perp c$).

field vector or oppositely. In the FC regime, below T_N the state is reached where the magnetic moment of subsystem M_{II} is directed along the magnetic field; correspondingly, the smaller magnetic moment of subsystem M_I is directed oppositely. The coercivity of subsystem M_I at these temperatures is small. As the temperature is decreased, the difference between these moments monotonically increases. The coercivity determined mainly by subsystem M_I also increases. In the ZFC regime, the moment of subsystem M_I, due to the shorter relaxation time, aligns along the magnetic field and specifies the growth of the moment of subsystem M_{II} in the opposite direction. This state with the resulting magnetic moment directed oppositely to the magnetic field is stable only at $T<T_{cr}$.

The $Mn_{1.2}Ni_{1.8}BO_5$ sample (Fig. 4b) in the ZFC regime undergoes a transition to the state with the positive magnetization at switching on of the magnetic field. With an increase in temperature, the magnetization decreases, passes the compensation point $M=0$, and near T_N turns to the FC state value. The magnetization pole reversal is observed only in weak magnetic fields (Fig. 9). Magnetic field dependences of the magnetization for this sample differ from those for $Mn_{2.5}Ni_{0.5}BO_5$ (Figs. 10 and 11). For $H \perp c$ and low temperatures, the hysteresis loops are strongly extended and the difference between their branches vanishes only in strong magnetic fields ($H=60$–70 kOe). As the temperature is increased, the loop shape changes and at $T=50$ K the loop is similar to that observed for $Mn_{2.5}Ni_{0.5}BO_5$. For $H \| c$, there is no hysteresis (Fig. 11).

In terms of crystal chemistry, the established features of the magnetic hysteresis of the $Mn_{1.2}Ni_{1.8}BO_5$ sample can be attributed to the higher degree of positional disordering of Ni^{2+}

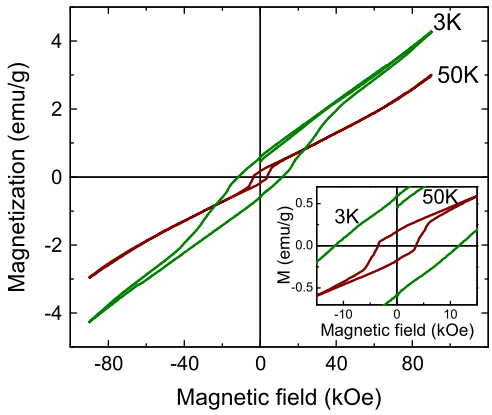

Fig. 10. Magnetic field dependences of magnetization of $Mn_{1.2}Ni_{1.8}BO_5$ measured at different temperatures ($H \perp c$).

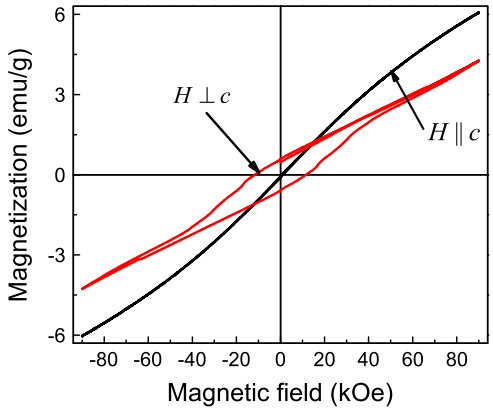

Fig. 11. Magnetic field dependences of magnetization of $Mn_{1.2}Ni_{1.8}BO_5$ measured at $H \perp c$ and $H \| c$ (T=3 K).

cations as compared with the $Mn_{2.5}Ni_{0.5}BO_5$ sample. These cations with strong spin–orbit coupling determine the spin–lattice interaction of the magnetic subsystems. Disordering of Ni^{2+} cations is accompanied by the formation of fragments with mutually misoriented easy axes in the ferrimagnetic phase. This yields the extended hysteresis loop in the low-temperature region. However, with an increase in temperature, the spin–lattice coupling weakens and the axis characteristic of the sample with low Ni concentration becomes predominant.

The model comprising two antiferromagnetically interacting subsystems each being ferrimagnetically ordered can be adapted to the $Mn_{1.2}Ni_{1.8}BO_5$ crystal. In this case, it is assumed that each subsystem in the model reveals the properties described in the previous section, the coercivities of the subsystems are comparable and the sign of the magnetization $M=M_I-M_{II}$ changes with temperature. In the FC regime, in the temperature region from Neel temperature T_N to compensation point T_{cr} the resulting magnetization is $M=M_I-M_{II}>0$ ($\chi>0$); below the compensation point, it is $M=M_I-M_{II}<0$ ($\chi<0$). In the ZFC regime, after switching on the magnetic field the state with $M=M_I-M_{II}>0$ ($\chi>0$) is stabilized. As the temperature is increased, the resulting magnetization below compensation point T_{cr} is $M=M_I-M_{II}<0$ ($\chi<0$). After that, at $T=T_{cr}$, the spin rotates by 180° and the crystal passes to the FC state (inset of Fig. 4). This transition is similar to the transition observed in the $Mn_{2.5}Ni_{0.5}BO_5$ sample in the ZFC regime at $H \perp c$. In both cases, spin reorientation occurs in the plane perpendicular to the c axis and is accompanied by the change in the magnetization sign. The magnetization pole reversal of the ferrimagnetic phase in the $Mn_{1.2}Ni_{1.8}BO_5$ sample is analogous to that observed on a powder sample of the Ni-containing antiferromagnet $Ni(HCOO)_2 \cdot 2H_2O$ [6].

5. Conclusions

The existence of the ludwigites $Mn_{3-x}Ni_xBO_5$ ($0<x<3$) with heterovalent Mn and Ni cations was established. Two qualitatively different scenarios in the behavior of the ferrimagnetic phases for the samples with the low ($x_1=0.5$) and high ($x_2=1.8$) Ni concentrations with the magnetization pole reversal were revealed. The possibility of describing these scenarios in the framework of the model comprising two antiferromagnetically interacting subsystems, each being ferrimagnetically ordered, was demonstrated.

To understand the correlation between these anomalies and the cation concentration in the ludwigite crystals, it is important to study the features of the magnetic behavior of the ludwigites $Mn_{3-x}Ni_xBO_5$ with $0.5<x<1.8$ and $x>3$.

Acknowledgments

The study was supported by the Siberian Branch of the Russian Academy of Sciencesintegration Project nos. 29 and 2.5.2.

References

[1] N. Menyuk, K. Dwight, et al., Phys. Rev. Lett. 4 (3) (1960) 119–120.
[2] Shin-ichi Ohkoshi, Abe Yukinori, et al., Phys. Rev. Lett. 82 (6) (1999) 1285–1288.
[3] Y. Ren, T.T.M. Palstra, et al., Nature 396 (1998) 441–444.
[4] O. Peña, K. Chanimi, et al., Bol. Soc. Esp. Ceram. 43 (3) (2004) 706–709.
[5] F. Bartolomé, J. Herrero-Albillos, et al., J. Appl. Phys. 97 (2005) 10A503.
[6] N. Inzaz, M. Boudard, et al., J. Alloys Compd. 479 (2009) 445–450.
[7] S.M. Yusuf, Amit Kumar, J.V. Yakhmi, Appl. Phys. Lett. 95 (2009) 182506.
[8] Amit Kumar, S.M. Yusuf, et al., Phys. Rev. Lett. 101 (2008) 207206.
[9] C. Mathonière, S.G. Garling, et al., J. Chem. Soc. Chem. Commun. (1994) 1551–1552.
[10] H. Kageyama, D.I. Khomskii, et al., Phys. Rev. B 67 (2003) 224422.
[11] L.N. Bezmaternykh, E.M. Kolesnikova et al., in: Proceedings of the Abstract volume of III International Conference on Crystallogenesis and Mineralogy, 2013, pp. 67–68.
[12] K. Bluhm, H.K. Müller-Buschbaum., Z. Anorg. Allg. Chem. 579 (1989) 111–115.
[13] G.M. Sheldrick, Acta Crystallogr. Sect. A 46 (1990) 467–473.